MATCH
Communications in Mathematical and in Computer Chemistry

MATCH Commun. Math. Comput. Chem. **94** (2025) 605–631
ISSN: 0340–6253
doi: 10.46793/match.94-3.04925

Spatiotemporal Oscillations of An Enzyme-Catalyzed Model

Xiaoyan Zhao[a], **Xue-Zhi Li**[b,c], **Mengxin Chen**[b,*]

[a] *Department of Basic Teaching, Henan Quality Engineering Vocational College, Pingdingshan, 467000, P. R. China*

[b] *School of Mathematics and Statistics , Henan Normal University, Xinxiang 453007, P. R. China*

[c] *School of Statistics and Mathematics, Henan Finance University, Zhengzhou 450046, P. R. China*

chmxdc@163.com (M. Chen)

(Received March 13, 2025)

Abstract

In this paper, we are committed to exploring the spatiotemporal oscillation behaviors of an enzyme-catalyzed model under no-flux boundary conditions. In the absence of spatial diffusion, we conduct stability analysis and establish the existence of Hopf bifurcation. Since the system admits periodic solutions when Hopf bifurcation occurs, we employ the multiple time scales (MTS) method to derive the amplitude equation, thereby determining the stability of the bifurcating periodic solutions. When diffusion is introduced, we examine the existence of Turing instabilities for the equilibrium and bifurcating periodic solution. Numerical simulations are utilized to validate the theoretical results. Our findings demonstrate that this enzyme-catalyzed model exhibits temporal, spatial, and spatiotemporal oscillations due to the presence of Hopf bifurcation, Turing instability, and Turing-Hopf bifurcation, respectively.

*Corresponding author.

1 Introduction

Spatial diffusion plays a crucial role in morphogenesis formation, leading to more complex dynamic behaviors across various systems, including population dynamics, disease transmission, chemical reactions, and biochemical processes. Numerous researchers have extensively studied reaction-diffusion models incorporating spatial diffusion, revealing intricate spatiotemporal dynamics. For detailed insights, please refer to [1–4].

Chemical and biochemical systems are widely utilized to simulate morphogenesis within spatial diffusion environments. Meanwhile, biochemical reaction systems represent a significant class of enzyme-catalyzed systems, often exhibiting complex nonlinear spatiotemporal phenomena. In this current paper, we are especially interested in the following diffusive non-dimensional version of the enzyme-catalyzed reaction system:

$$\begin{cases} \frac{\partial u}{\partial t} = d_1 \Delta u + \alpha - uv, & x \in \Omega, \quad t > 0, \\ \frac{\partial v}{\partial t} = d_2 \Delta v + \gamma v \left(u - \frac{1}{v+1} \right), & x \in \Omega, \quad t > 0, \\ \frac{\partial u}{\partial \nu} = \frac{\partial v}{\partial \nu} = 0, & x \in \partial\Omega, \quad t \geq 0, \\ u(x,0) = u_0(x) \geq 0, \quad v(x,0) = v_0(x) \geq 0, & x \in \Omega, \end{cases} \tag{1}$$

where $u = u(x,t)$ and $v = v(x,t)$ describe the concentrations of two distinct substrates, they are synthesized by enzyme-catalyzed reaction at space position x and reaction time t. Two parameters α and γ are positive kinetics constants. Additionally, $d_1 > 0$ and $d_2 > 0$ are diffusion rates and they describe the movement speeds of the substrates u and v, respectively. The notation Δ is the Laplacian operator in one-dimensional space and $\Omega = (0, \ell\pi) \subset \mathbb{R}$ with $\ell > 0$ is a bounded region with its smooth boundary $\partial\Omega$, ν presents an outward unit normal vector. We can recommend the papers [5–7] for the modified version and known dynamic analysis of (1).

By utilizing the enzyme-catalyzed reaction system (1), our primary objective is to investigate spatiotemporal oscillation behaviors through bifurcation method. Specifically, we establish the existence of Hopf bifurcation, Turing instability, and Hopf-Turing bifurcation for system (1). In the absence of diffusion and by selecting the parameter γ as the bifurcation control coefficient, we demonstrate the occurrence of Hopf bifurcation,

which directly leads to the emergence of bifurcating periodic solutions. A critical aspect of this analysis is determining the stability of these periodic solutions, a problem central to Hopf bifurcation theory. This stability problem is typically classified into two classical types: supercritical and subcritical. In the supercritical case, the bifurcating periodic solution is stable, whereas it is unstable in the subcritical case.

With the advancement of bifurcation theory, numerous techniques have been developed to study the direction of bifurcations, including center manifold reduction and normal form theory [8, 9], Crandall-Rabinowitz local bifurcation theory [10, 11], and Lyapunov-Schmidt reduction [12, 13], among others. In contrast to these established methods, we employ the multiple time scales (MTS) approach (cf. [2,14,15]) to derive the amplitude equation, thereby addressing the direction problem of the Hopf bifurcation. A notable feature of this approach is the separation of time into fast and slow scales through perturbation analysis. The amplitude equation for the Hopf bifurcation is then obtained by examining the perturbation equations associated with the slow time scale.

When spatial diffusion is introduced, we focus on the existence of Turing instability. It is worth noting that the Turing instability problem has been extensively studied in the literature due to its pivotal role in guiding the formation of spatial self-organization. For instance, Kumari et al. [15] demonstrated, based on a nutrient-phytoplankton system, that cross-diffusion significantly influences Turing instability. Similarly, Song et al. [16] highlighted that the local stability of a homogeneous equilibrium can be disrupted by either the topology of multiplex networks or cross-diffusion, leading to the formation of various Turing patterns. In [17], Chen and Fu explored the global existence and boundedness of solutions, revealing that prey evasion can drive Turing instability in predator-prey systems. Additionally, Manna and Banerjee [18] investigated Turing instability in an ecological system and derived the cubic Stuart-Landau equation near the instability threshold using weakly nonlinear analysis. For further insights into Turing instability, one may refer to the existing works [19–22] and the references therein. In this study, we not only investigate the emergence of Turing instability for the equilibrium but also analyze the

periodic solutions arising from Hopf bifurcation. Specifically, when Turing instability occurs in the periodic solution, we establish the existence of Hopf-Turing bifurcation. Through these bifurcation analyses, we identify spatially homogeneous periodic solutions, nonconstant steady states, and spatially nonhomogeneous periodic solutions in the enzyme-catalyzed reaction system (1). Furthermore, numerical experiments are conducted to visualize the spatiotemporal oscillations of the system (1).

The structure of this paper is organized as follows. In Sec. 2, we report the Hopf bifurcation for the local system. Section 3 establishes the existence of Turing instabilities for the unique equilibrium and the periodic solution. In Sec. 4, we validate our theoretical findings through numerical simulations. Finally, Sec. 5 summarizes the main conclusions of this study.

2 Hopf bifurcation

2.1 The existence

For the enzyme-catalyzedsystem (1), its local system can be written as:

$$\begin{cases} \frac{du}{dt} = \alpha - uv, \\ \frac{dv}{dt} = \gamma v \left(u - \frac{1}{v+1} \right). \end{cases} \tag{2}$$

Firstly, we are able to obtain the positive equilibrium, say $E^* = (u^*, v^*)$, of system (2). By direct compute, one yields

$$u^* = 1 - \alpha, \quad v^* = \frac{\alpha}{1-\alpha}, \quad 0 < \alpha < 1. \tag{3}$$

Accordingly, the Jacobian matrix at E^* is derived as follows:

$$J_0 = \begin{pmatrix} \frac{\alpha}{\alpha-1} & \alpha - 1 \\ \frac{\gamma\alpha}{1-\alpha} & \gamma\alpha(1-\alpha) \end{pmatrix}.$$

Naturally, the related characteristic equation is expressed below:

$$\lambda^2 - T_0(\gamma)\lambda + D_0(\gamma) = 0, \tag{4}$$

where $T_0(\gamma) = \gamma\alpha(1-\alpha) + \frac{\alpha}{\alpha-1}$ and $D_0(\gamma) = \gamma\alpha(1-\alpha) > 0$.

In light of (4), we build the following result.

Theorem 1. *Suppose that* $0 < \alpha < 1$ *is valid.*

(1) If $0 < \gamma < \frac{1}{(1-\alpha)^2}$*, then* E^* *is locally asymptotically stable;*

(2) If $\gamma > \frac{1}{(1-\alpha)^2}$*, then* E^* *is unstable;*

(3) If $\gamma := \gamma_H = \frac{1}{(1-\alpha)^2}$*, then system* (2) *enjoys the Hopf bifurcation.*

Proof. By utilizing (4), we can easily obtain the eigenvalues as follows:

$$\lambda_{1,2} = \frac{T_0(\gamma) \pm i\sqrt{4D_0(\gamma) - T_0^2(\gamma)}}{2} := \delta(\gamma) \pm iw(\gamma),$$

where

$$\delta(\gamma) = \mathbf{Re}\{\lambda_{1,2}\} = \frac{T_0(\gamma)}{2}, \quad w(\gamma) = \mathbf{Im}\{\lambda_{1,2}\} = \frac{\sqrt{4D_0(\gamma) - T_0^2(\gamma)}}{2}.$$

Owing to we have a fact that $D_0(\gamma) = \gamma\alpha(1-\alpha) > 0$, this implies $\mathbf{Re}\{\lambda_1\}$ and $\mathbf{Re}\{\lambda_2\}$ share the same sign, where $\mathbf{Re}\{\bullet\}$ denotes the real part of $\bullet$. We now discuss the stability of positive equilibrium E_* under different conditions. (1) If $0 < \gamma < \frac{1}{(1-\alpha)^2}$, then one has $T_0(\gamma) < 0$, namely, we have $\mathbf{Re}\{\lambda_1\} < 0$ and $\mathbf{Re}\{\lambda_2\} < 0$. Therefore, it is concluded that E^* is locally asymptotically stable. (2) If $\gamma > \frac{1}{(1-\alpha)^2}$, then we can infer that $T_0(\gamma) > 0$. For this case, there are $\mathbf{Re}\{\lambda_1\} > 0$ and $\mathbf{Re}\{\lambda_2\} > 0$. That is to say, the positive equilibrium E^* must be unstable. (3) If $\gamma := \gamma_H = \frac{1}{(1-\alpha)^2}$, it follows that $\mathbf{Re}\{\lambda_{1,2}\} = \delta(\gamma_H) = 0$ and $\mathbf{Im}\{\lambda_{1,2}\} = w(\gamma_H) = \sqrt{D_0(\gamma_H)} = \sqrt{\frac{\alpha}{1-\alpha}} > 0$, where $\mathbf{Im}\{\bullet\}$ describes the imaginary part of $\bullet$. Obviously, λ_1 and λ_2 are two purely imaginary eigenvalues of the characteristic equation (4). On the other hand, we can yield

$$\frac{d\mathbf{Re}\{\lambda_{1,2}\}}{d\gamma}\Big|_{\gamma=\gamma_H} = \frac{\alpha(1-\alpha)}{2} > 0. \tag{5}$$

In light of the Poincaré-Andronov-Hopf bifurcation theory, we can conclude that system (2) meets the Hopf bifurcation. We end the proof. ■

2.2 Direction of the Hopf bifurcation

It is observed that the local system (2) may undergo the Hopf bifurcation at a critical parameter value $\gamma = \gamma_H = \frac{1}{(1-\alpha)^2}$. Our subsequent objective is to determine the direction of this Hopf bifurcation using the multiple time scales (MTS) method. Now, we first reformulate system (2) as follows:

$$\frac{d\mathbf{U}}{dt} = J_0\mathbf{U} + N(\mathbf{U}, \mathbf{U}), \tag{6}$$

where $\mathbf{U} = (u, v)^T$ and

$$J_0 = \begin{pmatrix} \frac{\alpha}{\alpha-1} & \alpha - 1 \\ \frac{\gamma\alpha}{1-\alpha} & \gamma\alpha(1-\alpha) \end{pmatrix},$$

and

$$N = \begin{pmatrix} 0 \\ \gamma uv + \gamma(1-\alpha)^3v^2 - \gamma(1-\alpha)^4v^3 \end{pmatrix} + \mathcal{O}(4).$$

To apply the MTS approach, we shall do some perturbations with respect to ε. Suppose that $T_0 = t, T_2 = \varepsilon^2 t$ for $\varepsilon \ll 1$, which implies

$$\frac{\partial}{\partial t} = \frac{\partial}{\partial T_0} + \varepsilon^2 \frac{\partial}{\partial T_2}. \tag{7}$$

For the solution $\mathbf{U}$ of the problem (6), we assume the expansion

$$\mathbf{U} = \varepsilon \begin{pmatrix} u_1 \\ v_1 \end{pmatrix} + \varepsilon^2 \begin{pmatrix} u_2 \\ v_2 \end{pmatrix} + \varepsilon^3 \begin{pmatrix} u_3 \\ v_3 \end{pmatrix} + \mathcal{O}(4). \tag{8}$$

In addition, for N, we expand it as

$$N = \varepsilon^2 N_2 + \varepsilon^3 N_3 + \mathcal{O}(4), \tag{9}$$

where

$$N_2 = \begin{pmatrix} 0 \\ \gamma u_1 v_1 + \gamma(1-\alpha)^3 v_1^2 \end{pmatrix},$$

and

$$N_3 = \begin{pmatrix} 0 \\ \gamma(u_1v_2 + u_2v_1) + \gamma(1-\alpha)^3 v_1 v_2 - \gamma(1-\alpha)^4 v_1^3 \end{pmatrix}.$$

It is noticed that system (2) meets Hopf bifurcation at the point $\gamma = \gamma_H = \frac{1}{(1-\alpha)^2}$, so for $\varepsilon > 0$, we set $\gamma - \gamma_H = \varepsilon^2\delta$ with $\delta > 0$. As such, the matrix J_0 can be decomposed as

$$J_0 = \widehat{J}_0 + (\gamma - \gamma_H)M = \widehat{J}_0 + \varepsilon^2\delta M, \tag{10}$$

where

$$\widehat{J}_0 = \begin{pmatrix} \frac{\alpha}{\alpha-1} & \alpha - 1 \\ \frac{\gamma_H\alpha}{1-\alpha} & \gamma_H\alpha(1-\alpha) \end{pmatrix} = \begin{pmatrix} \frac{\alpha}{\alpha-1} & \alpha - 1 \\ \frac{\alpha}{(1-\alpha)^3} & \frac{\alpha}{1-\alpha} \end{pmatrix},$$

and

$$M = \begin{pmatrix} 0 & 0 \\ \frac{\alpha}{1-\alpha} & \alpha(1-\alpha) \end{pmatrix}.$$

In the following, we plan to submit (7)-(10) into (6). Then, we get

$\mathcal{O}(\varepsilon)$:

$$\frac{\partial}{\partial T_0}\begin{pmatrix} u_1 \\ v_1 \end{pmatrix} - \widehat{J}_0 \begin{pmatrix} u_1 \\ v_1 \end{pmatrix} = \mathbf{0}. \tag{11}$$

$\mathcal{O}(\varepsilon^2)$:

$$\frac{\partial}{\partial T_0}\begin{pmatrix} u_2 \\ v_2 \end{pmatrix} - \widehat{J}_0 \begin{pmatrix} u_2 \\ v_2 \end{pmatrix} = N_2. \tag{12}$$

$\mathcal{O}(\varepsilon^3)$:

$$\frac{\partial}{\partial T_0}\begin{pmatrix} u_3 \\ v_3 \end{pmatrix} - \widehat{J}_0 \begin{pmatrix} u_3 \\ v_3 \end{pmatrix} = -\frac{\partial}{\partial T_2}\begin{pmatrix} u_1 \\ v_1 \end{pmatrix} + \delta M \begin{pmatrix} u_1 \\ v_1 \end{pmatrix} + N_3. \tag{13}$$

Now, let us investigate the above three perturbation equations, respec-

tively. Recalling that the characteristic equation (4) has a pair purely imaginary roots $\lambda_{1,2} = \pm i\sqrt{D_0(\gamma_H)} = \pm i\sqrt{\frac{\alpha}{1-\alpha}} := \pm i\psi$ when $\gamma = \gamma_H = \frac{1}{(1-\alpha)^2}$, where $\psi = \sqrt{\frac{\alpha}{1-\alpha}}$. As a result, for the perturbation equation (11), we can consider the following general solution:

$$\begin{pmatrix} u_1 \\ v_1 \end{pmatrix} = A(T_2)\mathbf{v}e^{i\psi T_0} + \bar{A}(T_2)\bar{\mathbf{v}}e^{-i\psi T_0}, \tag{14}$$

where we assume that $A(T_2)$ is the complex amplitude and the eigenvector $\mathbf{v}$ takes the form $\mathbf{v} = (1, v_c)^T = \left(1, \frac{\psi(i+\psi)}{\alpha-1}\right)^T$. As such, (14) becomes

$$\begin{pmatrix} u_1 \\ v_1 \end{pmatrix} = A(T_2)\begin{pmatrix} 1 \\ v_c \end{pmatrix} e^{i\psi T_0} + \bar{A}(T_2)\begin{pmatrix} 1 \\ \bar{v}_c \end{pmatrix} e^{-i\psi T_0}.$$

Therefore, when $\gamma = \gamma_H$, we can get

$$N_2 = \begin{pmatrix} 0 \\ \gamma_H[A^2(T_2)v_c e^{2i\psi T_0} + |A(T_2)|^2 v_c] \\ +\gamma_H(1-\alpha)^3[(A^2(T_2)v_c^2 e^{2i\psi T_0} + |A(T_2)|^2|v_c|^2] \end{pmatrix} + c.c.,$$

where *c.c.* represents the conjugate terms. Keeping this in mind, we can assume that the particular solution to the problem (12) has the form

$$\begin{aligned} \begin{pmatrix} u_2 \\ v_2 \end{pmatrix} =& A^2(T_2)\begin{pmatrix} \vartheta_1 \\ \vartheta_2 \end{pmatrix} e^{2i\psi T_0} + \begin{pmatrix} \vartheta_3 \\ \vartheta_4 \end{pmatrix} |A(T_2)|^2 \\ &+ \bar{A}^2(T_2)\begin{pmatrix} \bar{\vartheta}_1 \\ \bar{\vartheta}_2 \end{pmatrix} e^{-2i\psi T_0}, \end{aligned} \tag{15}$$

where ϑ_j are undetermined for $j = 1, 2, 3, 4$. To compute ϑ_j, we are able to submit (15) into (12). Thereby, we get

$$\begin{aligned} \vartheta_1 =& -\frac{\gamma_H v_c J_{12}[1 + (1-\alpha)^3 v_c]}{3\psi^2}, \quad \vartheta_2 = -\frac{\gamma_H v_c(2i\psi - J_{11})[1 + (1-\alpha)^3 v_c]}{3\psi^2}, \\ \vartheta_3 =& \frac{\gamma_H v_c J_{12}[1 + (1-\alpha)^3 \bar{v}_c]}{\psi^2}, \quad \vartheta_4 = -\frac{\gamma_H v_c J_{11}[1 + (1-\alpha)^3 \bar{v}_c]}{\psi^2}, \end{aligned}$$

where $J_{11} = \frac{\alpha}{\alpha-1}$ and $J_{12} = \alpha - 1$. Using (14) and (15), one obtains

$$N_3 = \begin{pmatrix} 0 \\ \gamma_H[C_1 A^3(T_2)e^{3i\psi T_0} + C_2 A(T_2)|A(T_2)|^2 e^{i\psi T_0}] \\ +\gamma_H(1-\alpha)^3[\vartheta_2 v_c A^3(T_2)e^{3i\psi T_0} + (v_c\vartheta_4 + \bar{v}_c\vartheta_2)A(T_2)|A(T_2)|^2 e^{i\psi T_0}] \\ -\gamma_H(1-\alpha)^4[v_c^3 A^3(T_2)e^{3i\psi T_0} + 3v_c|v_c|^2 A(T_2)|A(T_2)|^2 e^{i\psi T_0}] \end{pmatrix} + c.c.,$$

where $C_1 = \vartheta_2 + \vartheta_1 v_c, C_2 = \vartheta_4 + \vartheta_2 + v_c\vartheta_3 + \bar{v}_c\vartheta_1$ and $c.c.$ is the conjugate term. Consequently, the perturbation (13) can be rewritten as follows:

$$\frac{\partial}{\partial T_0}\begin{pmatrix} u_3 \\ v_3 \end{pmatrix} - \widehat{J}_0 \begin{pmatrix} u_3 \\ v_3 \end{pmatrix} = \Phi e^{i\psi T_0} + \text{NST} + c.c., \tag{16}$$

where NST describes the non-secular terms and $\Phi = (\varphi_1, \varphi_2)^T$ with

$$\varphi_1 = -\frac{\partial A(T_2)}{\partial T_2}, \quad \varphi_2 = -v_c\frac{\partial A(T_2)}{\partial T_2} + C_3\delta A(T_2) + C_4 A(T_2)|A(T_2)|^2,$$

where $C_3 = \frac{\alpha[1+v_c(1-\alpha)^2]}{1-\alpha}$ and $C_4 = \gamma_H C_2 + \gamma_H(1-\alpha)^3(v_c\vartheta_4 + \bar{v}_c\vartheta_2) - 3\gamma_H(1-\alpha)^4 v_c|v_c|^2$. Taking $\mathbf{v}^\dagger = (v_c^\dagger, 1)^T = \left(\frac{\psi(i+\psi)}{1-\alpha}, 1\right)^T$, then (16) has non-zero solution only if the following Fredholm alternative condition is satisfied:

$$\left\langle \begin{pmatrix} v_c^\dagger \\ 1 \end{pmatrix}, \begin{pmatrix} \varphi_1 \\ \varphi_2 \end{pmatrix} \right\rangle = 0, \tag{17}$$

where the inner product is defined as $< a, b >= \frac{1}{\ell\pi}\int_0^{\ell\pi} \bar{a}^T b dx$. We obtain

$$(\bar{v}_c^\dagger + v_c)\frac{\partial A(T_2)}{\partial T_2} = \delta C_3 A(T_2) + C_4 A(T_2)|A(T_2)|^2. \tag{18}$$

For the Hopf bifurcation, we assume that each amplitude $A(T_2)$ in (18) takes the form $A(T_2) = ze^{-i\psi T_2}$ with $z = p + iq$. Hence, we can obtain

$$\begin{cases} \dot{p} = -\psi q + \delta(\mathbf{Re}\{C_5\}p - \mathbf{Im}\{C_5\}q) + (\mathbf{Re}\{C_6\}p - \mathbf{Im}\{C_6\}q)(p^2+q^2), \\ \dot{q} = \psi q + \delta(\mathbf{Re}\{C_5\}q - \mathbf{Im}\{C_5\}p) + (\mathbf{Re}\{C_6\}q - \mathbf{Im}\{C_6\}p)(p^2+q^2), \end{cases} \tag{19}$$

where

$$C_5 = \frac{C_3}{\bar{v}_c^{\dagger} + v_c}, \quad C_6 = \frac{C_4}{\bar{v}_c^{\dagger} + v_c}.$$

Applying the transformations $p = \rho\cos\theta$ and $q = \rho\sin\theta$, then (19) has the form

$$\begin{cases} \dot{\rho} = \rho(\delta\xi_1 + \xi_2\rho^2) + \mathcal{O}(\rho^4), \\ \dot{\theta} = \psi + \mathcal{O}(|\delta|, \rho^2), \end{cases} \tag{20}$$

where $\xi_1 = \mathbf{Re}\{C_5\}$ and $\xi_2 = \mathbf{Re}\{C_6\}$.

We should mention that (20) is the *amplitude equation* of the Hopf bifurcation bifurcation at the critical point $\gamma = \gamma_H$. The following result addresses the direction of the Hopf bifurcation by utilizing this amplitude equation.

Theorem 2. *Suppose that* $0 < \alpha < 1$ *is satisfied.*

(1) If $\xi_1\xi_2 > 0$*, no Hopf bifurcation occurs;*

(2) If $\xi_1\xi_2 < 0$*, the Hopf bifurcation may occur. Specifically, there is supercritical (resp. subcritical) Hopf bifurcation when* $\xi_1 > 0$ *(resp.* $\xi_1 < 0$*) and the bifurcating solution is stable (resp. unstable).*

Proof. The amplitude equation (20) admits a unique solution $\rho = \sqrt{\frac{-\delta\xi_1}{\xi_2}}$, which exists only when $\xi_1\xi_2 < 0$ is satisfied owing to $\delta > 0$. On the other hand, one claims that $-2\delta\xi_1$ is the unique eigenvalue of the amplitude equation (20). Keeping these in mind, the proof is completed. ■

Remark 1. We can obtain the precise expression of the amplitude $A(T_2)$ in (18).

$$A(T_2) = ze^{-i\psi T_2} = (p + iq)e^{-i\psi T_2} = (\rho\cos\theta + i\rho\sin\theta)e^{-i\psi T_2} = \rho e^{i(\theta - \psi T_2)},$$

where $\psi = \sqrt{\frac{\alpha}{1-\alpha}} > 0$. Note that $T_0 = t, T_2 = \varepsilon^2 t$, so one gets

$$A(T_2) = \rho e^{i(\theta - \psi T_2)} = \rho e^{i(\theta - \varepsilon^2\psi t)}.$$

The following pictures demonstrate that the influence of the amplitude

$A(T_2)$ on the parameter ε. Specifically, we fix $\rho = 0.01, \alpha = 0.38, \theta \in [0, 2\pi]$ and $t \in [0, 500]$. The numerical results indicate that the oscillation frequency of the amplitude $A(T_2)$ increases with the parameter ε within a fixed time interval, as depicted in Fig. 1.

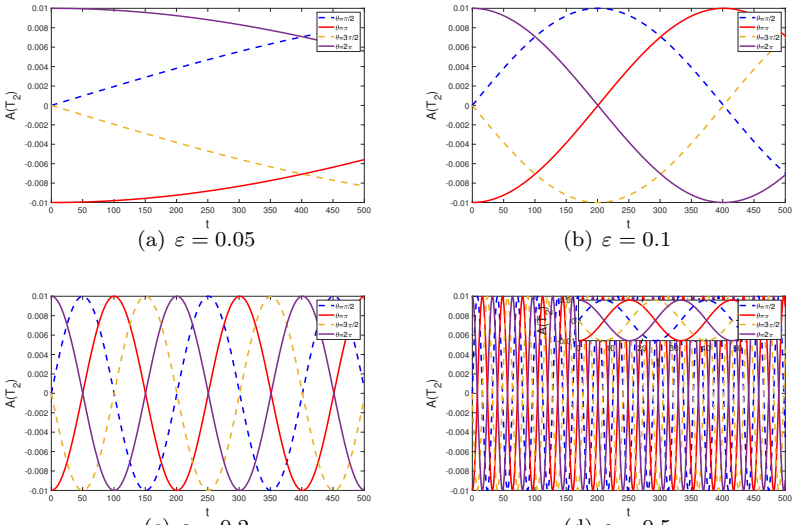

(a) $\varepsilon = 0.05$ (b) $\varepsilon = 0.1$

(c) $\varepsilon = 0.2$ (d) $\varepsilon = 0.5$

Figure 1. The oscillation frequency of the amplitude $A(T_2)$ against ε.

3 Turing instability

3.1 Turing instability of the equilibrium

Considering the local linearized system of the enzyme-catalyzed model (1):

$$\frac{\partial}{\partial t}\begin{pmatrix} u \\ v \end{pmatrix} = D\begin{pmatrix} u \\ v \end{pmatrix} + J_0\begin{pmatrix} u \\ v \end{pmatrix}, \tag{21}$$

where

$$D = \begin{pmatrix} d_1\Delta & 0 \\ 0 & d_2\Delta \end{pmatrix}, \quad J_0 = \begin{pmatrix} \frac{\alpha}{\alpha-1} & \alpha - 1 \\ \frac{\gamma\alpha}{1-\alpha} & \gamma\alpha(1-\alpha) \end{pmatrix}.$$

Considering the eigenvalue problem

$$\begin{cases} d_1\zeta_{xx} + \frac{\alpha}{\alpha-1}\zeta + (\alpha-1)\eta = \lambda_n\zeta, \\ d_2\eta_{xx} + \frac{\gamma\alpha}{1-\alpha}\zeta + \gamma\alpha(1-\alpha)\eta = \lambda_n\eta, \\ \frac{\partial\zeta}{\partial\nu} = \frac{\partial\eta}{\partial\nu} = 0, \end{cases} \tag{22}$$

where λ_n denote the eigenvalues of the problem (22) for $n \in \mathbb{N}_0 = \{0, 1, 2, \cdots\}$. Moreover, $\zeta(x)$ and $\eta(x)$ are eigenfunctions of (22) and they have the form:

$$\zeta(x) = \sum_{n=0}^{\infty} a_n \cos\frac{nx}{\ell}, \quad \eta(x) = \sum_{n=0}^{\infty} b_n \cos\frac{nx}{\ell},$$

where a_n and b_n are set to be non-zero constants. By using (22), one has

$$\sum_{n=0}^{\infty}(J_n - \lambda_n I)\begin{pmatrix} a_n \\ b_n \end{pmatrix}\cos\frac{nx}{\ell} = 0,$$

where

$$J_n = \begin{pmatrix} \frac{\alpha}{\alpha-1} - d_1\frac{n^2}{\ell^2} & \alpha-1 \\ \frac{\gamma\alpha}{1-\alpha} & \gamma\alpha(1-\alpha) - d_2\frac{n^2}{\ell^2} \end{pmatrix}.$$

In this fashion, one obtains the characteristic equation as follows:

$$\lambda_n^2 - T_n(\gamma, d_2)\lambda_n + D_n(\gamma, d_2) = 0, \text{ for } n \in \mathbb{N}_0 = \{0, 1, 2, \cdots\}, \tag{23}$$

where

$$\begin{cases} T_n(\gamma, d_2) = -(d_1 + d_2)\frac{n^2}{\ell^2} + \frac{\alpha}{\alpha-1} + \gamma\alpha(1-\alpha), \\ D_n(\gamma, d_2) = d_1 d_2\frac{n^4}{\ell^4} - \left[\frac{\alpha}{\alpha-1}d_2 + \gamma\alpha(1-\alpha)d_1\right]\frac{n^2}{\ell^2} + \gamma\alpha(1-\alpha), \end{cases}$$

To obtain the occurrence conditions of the Turing instability of the enzyme-catalyzedsystem (1), one requires the unique equilibrium E^* is locally asymptotically stable for spatially homogeneous local system (2). To that end, in light of Theorem 1, there must holds

$$0 < \gamma < \gamma_H, \quad \gamma_H = \frac{1}{(1-\alpha)^2}. \tag{24}$$

Remember this restriction, we discuss the following four cases by considering the ranges of the diffusion rates d_1 and d_2 in (1).

Case 1. $d_1 = d_2 = d$.

If $d_1 = d_2 = d$ holds, we can get $T_n(\gamma, d_2) = -2d\frac{n^2}{\ell^2} + \frac{\alpha}{\alpha-1} + \gamma\alpha(1-\alpha) < 0$ and $D_n(\gamma, d_2) = d^2\frac{n^4}{\ell^4} - d\left[\frac{\alpha}{\alpha-1} + \gamma\alpha(1-\alpha)\right]\frac{n^2}{\ell^2} + \gamma\alpha(1-\alpha)$. Because $T_n(\gamma, d_2) < 0$ for any $n \in \mathbb{N}_0$, the stability of E^* uniquely determined by the sign of $D_n(\gamma, d_2)$. In precise, if $D_n(\gamma, d_2) > 0$, then all real parts of eigenvalues of (23) are negative. This implies that the unique equilibrium E^* is locally asymptotically stable. If $D_n(\gamma, d_2) < 0$, then at least one eigenvalue of (23) with positive real part. For this case, the unique equilibrium E^* is unstable in Turing sense. Recalling (24), one yields $\frac{\alpha}{\alpha-1} + \gamma\alpha(1-\alpha) = -\frac{\alpha}{1-\alpha} + \gamma\alpha(1-\alpha) < -\frac{\alpha}{1-\alpha} + \gamma_H\alpha(1-\alpha) = 0$. Accordingly, for any $n \in \mathbb{N}_0$, we can infer that $D_n(\gamma, d_2) = d^2\frac{n^4}{\ell^4} - d\left[\frac{\alpha}{\alpha-1} + \gamma\alpha(1-\alpha)\right]\frac{n^2}{\ell^2} + \gamma\alpha(1-\alpha) > d^2\frac{n^4}{\ell^4} + \gamma\alpha(1-\alpha) > 0$. Hence, E^* is locally asymptotically stable. Of course, there is no Turing instability.

Case 2. $0 < d_1 < d_2$.

If $0 < d_1 < d_2$ is satisfied, we can first immediately obtain $T_n(\gamma, d_2) = -(d_1+d_2)\frac{n^2}{\ell^2} + \frac{\alpha}{\alpha-1} + \gamma\alpha(1-\alpha) < 0$ for any $n \in \mathbb{N}_0$. Utilizing (24), one has $\frac{\alpha}{\alpha-1}d_2 + \gamma\alpha(1-\alpha)d_1 < \frac{\alpha}{\alpha-1}d_2 + \gamma\alpha(1-\alpha)d_2 < \frac{\alpha}{\alpha-1}d_2 + \gamma_H\alpha(1-\alpha)d_2 = 0$. So, we can deduce that $D_n(\gamma, d_2) = d_1d_2\frac{n^4}{\ell^4} - \left[\frac{\alpha}{\alpha-1}d_2 + \gamma\alpha(1-\alpha)d_1\right]\frac{n^2}{\ell^2} + \gamma\alpha(1-\alpha) > d_1d_2\frac{n^4}{\ell^4} + \gamma\alpha(1-\alpha) > 0$. Hence, E^* is locally asymptotically stable and there is no Turing instability.

Case 3. $0 < d_1 \leq \frac{1}{\gamma(1-\alpha)^2}d_2$.

Obviously, there holds $T_n(\gamma, d_2) = -(d_1+d_2)\frac{n^2}{\ell^2} + \frac{\alpha}{\alpha-1} + \gamma\alpha(1-\alpha) < 0$ for any $n \in \mathbb{N}_0$. Now, if $0 < d_1 \leq \frac{1}{\gamma(1-\alpha)^2}d_2$ is valid, we can immediately obtain a fact that $\frac{\alpha}{\alpha-1}d_2 + \gamma\alpha(1-\alpha)d_1 \leq 0$. As a consequence, one has $D_n(\gamma, d_2) = d_1d_2\frac{n^4}{\ell^4} - \left[\frac{\alpha}{\alpha-1}d_2 + \gamma\alpha(1-\alpha)d_1\right]\frac{n^2}{\ell^2} + \gamma\alpha(1-\alpha) \geq d_1d_2\frac{n^4}{\ell^4} + \gamma\alpha(1-\alpha) > 0$ for any $n \in \mathbb{N}_0$. For this case, E^* is locally asymptotically stable and there is no Turing instability.

Case 4. $d_1 > \frac{1}{\gamma(1-\alpha)^2}d_2$.

If $d_1 > \frac{1}{\gamma(1-\alpha)^2}d_2$ is true, we know that $\frac{\alpha}{\alpha-1}d_2 + \gamma\alpha(1-\alpha)d_1 > 0$.

Denote by $z := n^2/\ell^2$ and let

$$f(z) := d_1 d_2 z^2 - \left[\frac{\alpha}{\alpha - 1} d_2 + \gamma\alpha(1-\alpha)d_1\right] z + \gamma\alpha(1-\alpha), \quad z > 0.$$

Clearly, we have $D_n(\gamma, d_2) = f(z)$ with $z = n^2/\ell^2$. In what follows, let us discuss the sign of $f(z)$ for $z > 0$. Considering $\min_{z>0} f(z) = 0$, this is $\min_{z>0} f(z) = -\frac{\chi(d_2)}{4d_1 d_2} = 0$, where

$$\chi(d_2) := \frac{\alpha^2}{(\alpha-1)^2} d_2^2 - 2\gamma\alpha(2-\alpha)d_1 d_2 + \gamma^2\alpha^2(1-\alpha)^2 d_1^2.$$

Accordingly, we can obtain the root's existence criterion say $\Delta_{\chi(d_2)}$ of $\chi(d_2) = 0$ is $\Delta_{\chi(d_2)} = 16\gamma^2\alpha^2 d_1^2(1-\alpha)$. It is noticed that we have restricted $0 < \alpha < 1$ for the existence of E^*, one has $\Delta_{\chi(d_2)} = 16\gamma^2\alpha^2 d_1^2(1-\alpha) > 0$. It follows that $\chi(d_2) = 0$ has two different positive real roots, say $d_2^{(1)}$ and $d_2^{(2)}$, where

$$d_2^{(1)} = \frac{\gamma(2-\alpha)(\alpha-1)^2 - 2\gamma(\alpha-1)^2\sqrt{1-\alpha}}{\alpha} d_1 \tag{25}$$

and

$$d_2^{(2)} = \frac{\gamma(2-\alpha)(\alpha-1)^2 + 2\gamma(\alpha-1)^2\sqrt{1-\alpha}}{\alpha} d_1.$$

Note that $d_1 > \frac{1}{\gamma(1-\alpha)^2} d_2$, namely, $0 < d_2 < \gamma(1-\alpha)^2 d_1$, we can verify that

$$d_2^{(1)} - \gamma(1-\alpha)^2 d_1 = \frac{2\gamma(1-\alpha)(\alpha-1)^2 - 2\gamma(\alpha-1)^2\sqrt{1-\alpha}}{\alpha} d_1 < 0$$

and

$$d_2^{(2)} - \gamma(1-\alpha)^2 d_1 = \frac{2\gamma(1-\alpha)(\alpha-1)^2 + 2\gamma(\alpha-1)^2\sqrt{1-\alpha}}{\alpha} d_1 > 0.$$

Therefore, one obtains $d_2^{(1)} < \gamma(1-\alpha)^2 d_1 < d_2^{(2)}$. Keeping this in mind, it is concluded that $\chi(d_2) > 0$ as $d_2 \in \left(0, d_2^{(1)}\right)$ and $\chi(d_2) \leq 0$ when $d_2 \in \left[d_2^{(1)}, \gamma(1-\alpha)^2 d_1\right)$. Recalling that $\min_{z>0} f(z) = -\frac{\chi(d_2)}{4d_1 d_2}$ and $D_n(\gamma, d_2) =$

$f(z)$ with $z = n^2/\ell^2$, we know that the unique positive equilibrium E^* is locally asymptotically stable when $d_2 \in \left[d_2^{(1)}, \gamma(1-\alpha)^2 d_1\right)$ and it becomes unstable and there is Turing instability when $d_2 \in \left(0, d_2^{(1)}\right)$. In the sequel, let us determine the critical wave number, say n_T, for the Turing instability. Using the critical condition $\min_{z>0} f(z) = 0$ again and letting $d_2 = d_2^{(1)}$, we can get

$$n_T^2 = \frac{\alpha\ell^2}{d_1\sqrt{(2-\alpha)(1-\alpha) - 2(1-\alpha)\sqrt{1-\alpha}}} > 0. \tag{26}$$

We summarize these results as follows.

Theorem 3. *(Turing instability of equilibrium) Assume that* $0 < \gamma < \frac{1}{(1-\alpha)^2}$.

(1) If $0 < \alpha < 1$ *and* $0 < d_1 \le d_2$, *then* E^* *is locally asymptotically stable and no Turing instability occurs;*

(2) If $0 < \alpha < 1$ *and* $0 < d_1 \le \frac{1}{\gamma(1-\alpha)^2} d_2$, *then* E^* *is locally asymptotically stable and no Turing instability occurs;*

(3) If $0 < \alpha < 1$ *and* $d_2 \in \left[d_2^{(1)}, \gamma(1-\alpha)^2 d_1\right)$, *then* E^* *is locally asymptotically stable. However, if* $0 < \alpha < 1$ *and* $d_2 \in \left(0, d_2^{(1)}\right)$, *then* E^* *becomes unstable and there is Turing instability with the critical number* $n = n_T$, *where* $d_2^{(1)}$ *and* n_T *have been defined in* (25) *and* (26), *respectively.*

3.2 Turing instability of bifurcating periodic solution

Utilizing part (3) of Theorem 1, we deduce that the Hopf bifurcation occurs when $\gamma = \gamma_H = \frac{1}{(1-\alpha)^2}$, leading to the emergence of the periodic solution. Now, we want to explore the Turing instability of the periodic solution in the presence of diffusion. When $\gamma = \gamma_H = \frac{1}{(1-\alpha)^2}$, we can rewrite system (1) as follows:

$$\begin{cases} \frac{\partial u}{\partial t} = d_1\Delta u + \alpha - uv, & x \in \Omega, \quad t > 0, \\ \frac{\partial v}{\partial t} = d_2\Delta v + \frac{v}{(1-\alpha)^2}\left(u - \frac{1}{v+1}\right), & x \in \Omega, \quad t > 0, \\ \frac{\partial u}{\partial \nu} = \frac{\partial v}{\partial \nu} = 0, & x \in \partial\Omega, \quad t \ge 0, \\ u(x,0) = u_0(x) \ge 0, \quad v(x,0) = v_0(x) \ge 0, & x \in \Omega. \end{cases}$$

As we have discussed before, at the Hopf bifurcation critical point $\gamma = \gamma_H = 1/(1-\alpha)^2$, the corresponding characteristic equation takes the form:

$$\lambda_n^2 - T_n(\gamma_H, d_2)\lambda_n + D_n(\gamma_H, d_2) = 0, \text{ for } n \in \mathbb{N}_0 = \{0, 1, 2, \cdots\}, \quad (27)$$

where

$$\begin{cases} T_n(\gamma_H, d_2) = -(d_1 + d_2)\frac{n^2}{\ell^2}, \\ D_n(\gamma_H, d_2) = d_1 d_2 \frac{n^4}{\ell^4} - \frac{\alpha}{1-\alpha}(d_1 - d_2)\frac{n^2}{\ell^2} + \frac{\alpha}{1-\alpha}. \end{cases}$$

We also have two cases to discuss the stability of the periodic solution.

Case 1. $0 < d_1 \le d_2$.

If $0 < d_1 \le d_2$ is satisfied, clearly, we have $T_n(\gamma_H, d_2) = -(d_1+d_2)\frac{n^2}{\ell^2} < 0$ and $D_n(\gamma_H, d_2) = d_1 d_2 \frac{n^4}{\ell^4} - \frac{\alpha}{1-\alpha}(d_1 - d_2)\frac{n^2}{\ell^2} + \frac{\alpha}{1-\alpha} \ge d_1 d_2 \frac{n^4}{\ell^4} + \frac{\alpha}{1-\alpha} > 0$ for any $n \in \mathbb{N}_0 \backslash \{0\}$. This means that the periodic solution resulting from the Hopf bifurcation is stable and there is no Turing instability.

Case 2. $d_1 > d_2$.

If $d_1 > d_2$ is true, we denote by $p := n^2/\ell^2$ and let

$$f(p) := d_1 d_2 p^2 - \frac{\alpha}{1-\alpha}(d_1 - d_2)p + \frac{\alpha}{1-\alpha}, \quad p > 0.$$

That is to say, $D_n(\gamma_H, d_2) = f(p)$ with $p = n^2/\ell^2$. In a similar fashion, we should discuss the sign of $f(p)$ for $p > 0$ to obtain the existence conditions of the Turing instability of the periodic solution. Considering $\min_{p>0} f(p) = 0$, this is $\min_{p>0} f(p) = -\frac{\tau(d_2)}{4d_1 d_2} = 0$, where

$$\tau(d_2) := \alpha d_2^2 - 2(2-\alpha)d_1 d_2 + \alpha d_1^2.$$

It is easy to yield the root's existence criterion say $\Delta_{\tau(d_2)}$ of $\tau(d_2) = 0$ is $\Delta_{\tau(d_2)} = 16d_1^2(1-\alpha)$. Obviously, $\Delta_{\tau(d_2)} = 16d_1^2(1-\alpha) > 0$ is valid since $0 < \alpha < 1$. As such, $\tau(d_2) = 0$ enjoys two different positive real solutions, say d_2^* and d_2°, where

$$d_2^* = \frac{2 - \alpha - 2\sqrt{1-\alpha}}{\alpha} d_1, \quad d_2^\circ = \frac{2 - \alpha + 2\sqrt{1-\alpha}}{\alpha} d_1. \quad (28)$$

It is easy to check that $d_2^* < d_1$ and $d_2^\circ > d_1$ for $0 < \alpha < 1$. However,

one requires $d_1 > d_2$, so there must holds $\tau(d_2) > 0$ as $d_2 \in (0, d_2^*)$ and $\tau(d_2) \leq 0$ when $d_2 \in [d_2^*, d_1)$. It is noticed that $\min_{p>0} f(p) = -\frac{\tau(d_2)}{4d_1 d_2}$ and $D_n(\gamma_H, d_2) = f(p)$ with $p = n^2/\ell^2$, we can infer that the periodic solution keeps its stability when $d_2 \in [d_2^*, d_1)$ and it becomes unstable (in Turing sense) when $d_2 \in (0, d_2^*)$. In the sequel, let us determine the critical wave number, say n_{T^*}, for the Turing instability of the periodic solution. By employing $\min_{p>0} f(p) = 0$ again, we get

$$n_{T^*}^2 = \frac{\alpha \ell^2}{d_1 \sqrt{(2-\alpha)(1-\alpha) - 2(1-\alpha)\sqrt{(1-\alpha)}}} > 0. \tag{29}$$

In conclusion, we can have the following.

Theorem 4. *(Turing instability of bifurcating periodic solution) Suppose that* $0 < \alpha < 1$ *and* $\gamma = \gamma_H = 1/(1-\alpha)^2$ *are satisfied.*

(1) The periodic solution resulting from the Hopf bifurcation is stable when $0 < d_1 \leq d_2$*;*

(2) The periodic solution bifurcating from the Hopf bifurcation is stable when $d_2 \in [d_2^*, d_1)$*, whereas for* $d_2 \in (0, d_2^*)$*, it is Turing unstable with the wave number* $n = n_{T^*}$*;*

(3) The enzyme-catalyzed system (1) *undergoes the Hopf-Turing bifurcation when* $(\gamma, d_2) = (\gamma_H, d_2^*)$*, where* d_2^* *and* $n = n_{T^*}$ *can be found in* (28) *and* (29)*, respectively.*

Proof. Conclusions (1) and (2) follow directly from the previous analysis and computations. Benefitting from (3) of Theorem 1, one claims that the local system of (1) exhibits the Hopf bifurcation (0-mode). By employing part (3) of Theorem 3, we know that enzyme-catalyzed system (1) experiences the Turing bifurcation when $d_2 = d_2^{(1)}$ and $d_2^{(1)} = d_2^*$ as $\gamma = \gamma_H$. On the other hand, we shall perform the transversality condition of the Hopf-Turing bifurcation. To do so, we differentiate the control parameter d_2 of (23), one has

$$\frac{d\mathbf{Re}\{\lambda_n\}}{dd_2}\Big|_{\gamma=\gamma_H, d_2=d_2^*} = -\frac{d_1 \frac{n^2}{\ell^2} + \frac{\alpha}{1-\alpha}}{d_1 + d_2^*} < 0.$$

Combining this condition with $d_2^* = d_2^{(1)}$ as $\gamma = \gamma_H$. We end the proof. ■

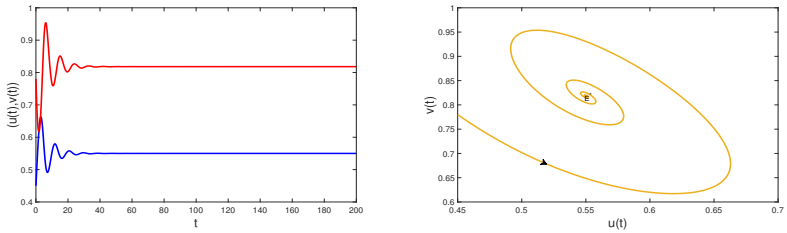

Figure 2. The equilibrium $E^* = (0.5500, 0.8182)$ is locally asymptotically stable for system (2), where $\alpha = 0.45$ and $\gamma = 2.5$.

4 Numerical simulation

In this section, we perform numerical simulations to validate the theoretical results established in Theorems 1-4.

Firstly, we are able to fix the parameter $\alpha = 0.45$, yielding the equilibrium $E^* = (0.5500, 0.8182)$ and the threshold of the Hopf bifurcation $\gamma_H = \frac{1}{(1-\alpha)^2} = 3.3058$. Now, we select the control parameter $2.5 = \gamma < \gamma_H$. Therefore, we can observe that $E^* = (0.5500, 0.8182)$ is locally asymptotically stable for system (2), as shown in Fig. 2. This figure confirms the effectiveness of Theorem 1.

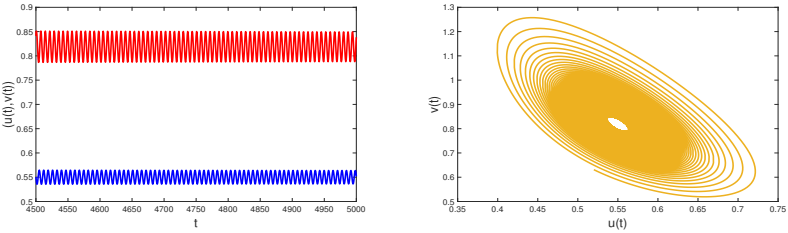

Figure 3. The stable periodic solution emerges in (2) owing to the supercritical Hopf bifurcation, where $\alpha = 0.45$ and $\gamma = 3.3058$.

Theorem 2 addresses the direction issue of the Hopf bifurcation. In fact, we particularly focus on the supercritical type of Hopf bifurcation,

as it leads to the stable bifurcating periodic solution. To achieve that, let us continuous choose $\alpha = 0.45$, one can yield $E^* = (0.5500, 0.8182)$ and the critical point of the Hopf bifurcation is $\gamma_H = \frac{1}{(1-\alpha)^2} = 3.3058$. Additionally, one obtains $C_5 = 0.1238 + 0.1368i$ and $C_6 = -1.0873 - 2.4374i$. Hence, we get $\xi_1 = \mathbf{Re}\{C_5\} = 0.1238 > 0$ and $\xi_2 = \mathbf{Re}\{C_6\} = -1.0873$. According to part (2) of Theorem 2, supercritical Hopf bifurcation emerges, resulting in the stable periodic solution. This theoretical prediction has been checked by Fig. 3.

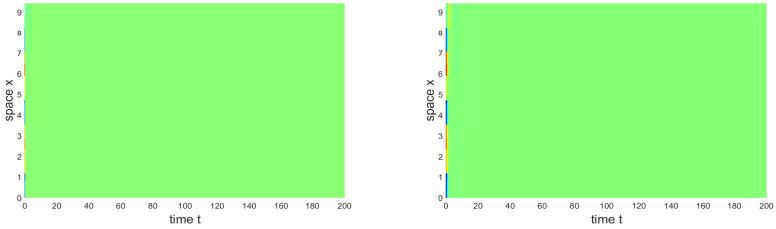

Figure 4. The equilibrium $E^* = (0.5, 1.0)$ is stable when $\ell = 3, \alpha = 0.5, \gamma = 2$ and $d_1 = d_2 = 0.75$.

In what follows, we are ready to confirm the theoretical conclusions given in Theorem 3 and Theorem 4, respectively. To this end, we shall fix $\ell = 3, \alpha = 0.5, \gamma = 2$ and $d_1 = d_2 = 0.75$. Then our numerical result shows that $E^* = (0.5, 1.0)$ is stable, see Fig. 4 for details. Hence, part (1) of Theorem 3 is true. Now, one chooses $\ell = 3, \alpha = 0.5, \gamma = 2$ and $d_2 = 0.5$. Accordingly, we get $\frac{1}{\gamma(1-\alpha)^2} d_2 = 1$. To fulfill part (2) of Theorem 3, we take the diffusion parameter $d_1 = 0.85$. Then our numerical result demonstrates that $E^* = (0, 5, 1.0)$ is stable, as depicted in Fig. 5. That is to say, part (2) of Theorem 3 is true. To proceed with our numerical experiments, we take $\ell = 3, \alpha = 0.5, \gamma = 2$ and $d_1 = 0.85$. In this fashion, one obtains

$$d_2^{(1)} = \frac{\gamma(2-\alpha)(\alpha-1)^2 - 2\gamma(\alpha-1)^2\sqrt{1-\alpha}}{\alpha} d_1 = 0.0729.$$

If we keep the diffusion coefficient $0.02 = d_2 < d_2^{(1)}$, then part (3) of Theorem 3 is satisfied. For this case, the enzyme-catalyzed system (1) suffers

from the Turing instability at the equilibrium $E^* = (0.5, 1.0)$. We can confirm this judgment, as shown in Fig. 6. It is clear that the equilibrium $E^* = (0.5, 1.0)$ becomes unstable because the existence of Turing instability. The corresponding phase trajectory diagram of Fig. 6 has been plotted in Fig. 7. It is revealed that enzyme-catalyzed system (1) admits spatial oscillation.

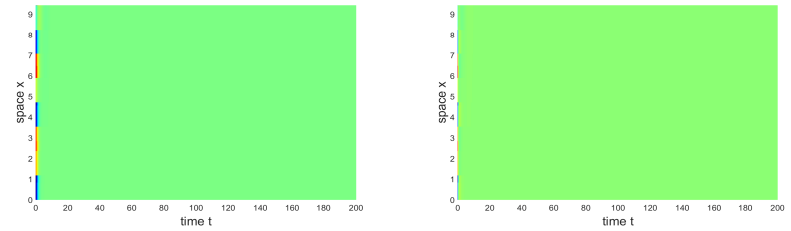

Figure 5. The equilibrium $E^* = (0.5, 1.0)$ is stable when $\ell = 3, \alpha = 0.5, \gamma = 2, d_1 = 0.85$ and $d_2 = 0.5$.

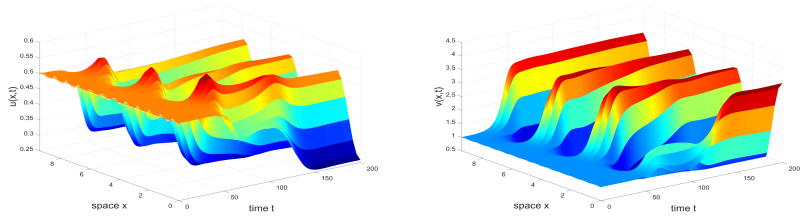

Figure 6. The equilibrium $E^* = (0.5, 1.0)$ becomes unstable because the existence of Turing instability, where $\ell = 3, \alpha = 0.5, \gamma = 2, d_1 = 0.85$ and $d_2 = 0.02$.

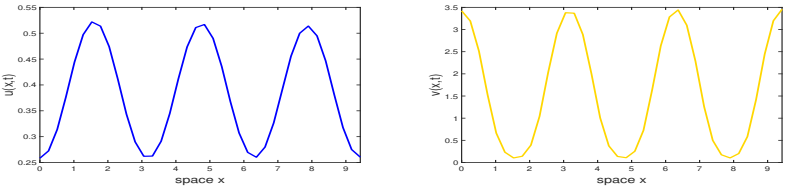

Figure 7. The corresponding phase trajectory diagram of Fig. 6. It shows that enzyme-catalyzed system (2) admits spatial oscillation, where $\ell = 3, \alpha = 0.5, \gamma = 2, d_1 = 0.85$ and $d_2 = 0.02$.

It is noticed that Hopf bifurcation occurs when the parameter γ reaches its critical value γ_H, we also want to explore the bifurcating solution of the enzyme-catalyzed system (1) at this point. To that end, one takes $\alpha = 0.45$, which yields $\gamma_H = \frac{1}{(1-\alpha)^2} = 3.3058$. Meanwhile, we take $\gamma = 3.3058, d_1 = 1.65$, then we can compute the critical diffusion coefficient

$$d_2^* = \frac{2 - \alpha - 2\sqrt{1-\alpha}}{\alpha} d_1 = 0.2448.$$

By selecting $0.85 = d_2$, which is greater than d_2^*. Numerical result demonstrates the emergence of the bifurcating solution in the enzyme-catalyzed system (1). Specifically, this solution represents the stable spatially homogeneous periodic solution, as illustrated in Fig. 8. The corresponding phase trajectory diagram of Fig. 8 has been presented in Fig. 9. We can observe that enzyme-catalyzed system (1) exhibits temporal oscillation.

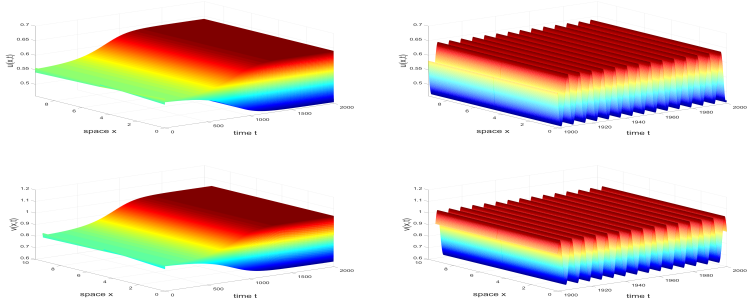

Figure 8. The enzyme-catalyzed system (1) admits the spatially homogeneous periodic solution, where $\alpha = 0.45, \gamma = 3.3058, d_1 = 1.65$ and $d_2 = 0.85$.

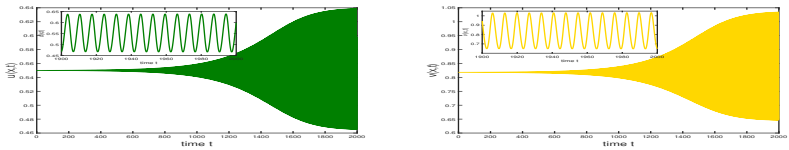

Figure 9. The corresponding phase trajectory diagram of Fig. 8. It shows enzyme-catalyzed system (2) admits temporal oscillation, where $\alpha = 0.45, \gamma = 3.3058, d_1 = 1.65$ and $d_2 = 0.85$.

As clearly demonstrated in Fig. 8, the system exhibits a spatially homogeneous periodic solution resulting from the Hopf bifurcation. Our subsequent numerical investigation reveals that this spatially homogeneous periodic solution transitions into a spatially nonhomogeneous periodic solution due to the emergence of Turing instability. Specifically, maintaining the parameters $\alpha = 0.45, \gamma = 3.3058, d_1 = 1.65$ as in Fig. 8, we select $0.233 = d_2$ which is below the critical value $d_2^* = 0.2448$. This parameter choice leads to the formation of a spatially nonhomogeneous periodic solution in the enzyme-catalyzed system (1), as illustrated in Fig. 10. The corresponding phase trajectory diagram is presented in Fig. 11, confirming that the enzyme-catalyzed system (1) exhibits spatiotemporal oscillations. The selected parameter pair $(\gamma, d_2) = (3.3058, 0.233)$ lies in close proximity to the Hopf-Turing bifurcation critical point $(\gamma, d_2) = (\gamma_H, d_2^*) = (3.3058, 0.2448)$. This strategic parameter selection enables us to observe the transition between different dynamical regimes. The numerical results presented in Fig. 8 and Fig. 10 provide strong evidence supporting the validity of statement (2) in Theorem 4.

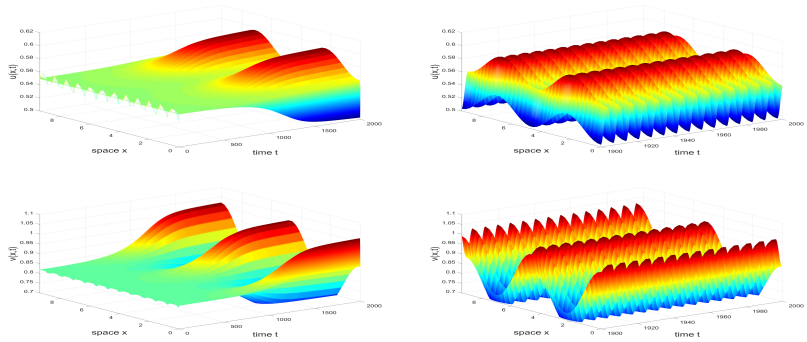

Figure 10. The enzyme-catalyzed system (1) admits the spatially nonhomogeneous periodic solution, where $\alpha = 0.45, \gamma = 3.3058, d_1 = 1.65$ and $d_2 = 0.233$.

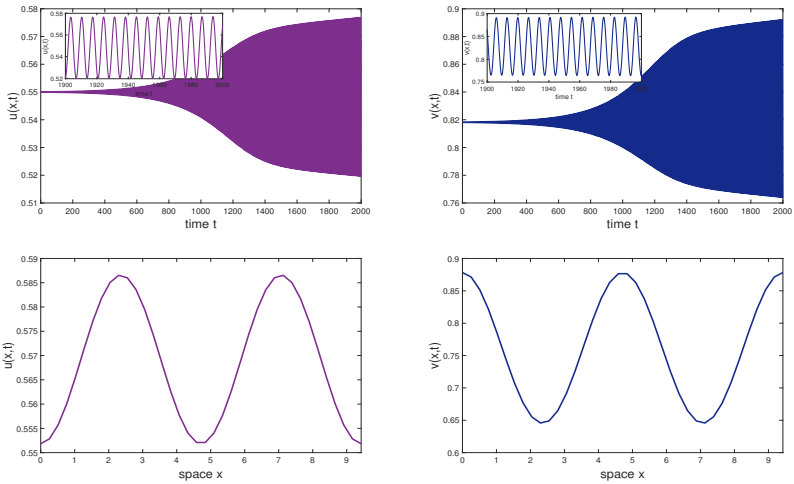

Figure 11. The corresponding phase trajectory diagram of Fig. 10. It is shown that enzyme-catalyzed system (1) admits spatiotemporal oscillation, where $\alpha = 0.45, \gamma = 3.3058, d_1 = 1.65$ and $d_2 = 0.233$.

Spatial Scale Effects on Reaction Oscillations. The influence of spatial scale on reaction oscillations is systematically investigated for the enzyme-catalyzed system (1). We consider the system defined on the domain $\Omega = (0, \ell\pi) \subset \mathbb{R}$ with $\ell > 0$ represents the spatial scale parameter. Through numerical simulations with fixed parameters $\alpha = 0.38, \gamma = 2.6, d_1 = 1.65$ and $d_2 = 0.173$, we examine the system's oscillatory behavior across different spatial scales. When taking spatial scales $\ell = 20, 30, 40$, the system exhibits stable spatial oscillations, as illustrated in panels (a)-(c) of Fig. 12. However, when extending the spatial scale to $\ell = 50$, a notable transition occurs: the system develops bistable spatial oscillations characterized by distinct amplitudes, shown in panel (d) of Fig. 12. This bistable behavior persists at larger spatial scales, as demonstrated in panels (e) and (f) for $\ell = 60$ and $\ell = 70$, respectively. These results clearly demonstrate that the spatial scale significantly influences the reaction oscillations in the enzyme-catalyzed system (1), particularly through the emergence of amplitude-dependent bistable oscillations.

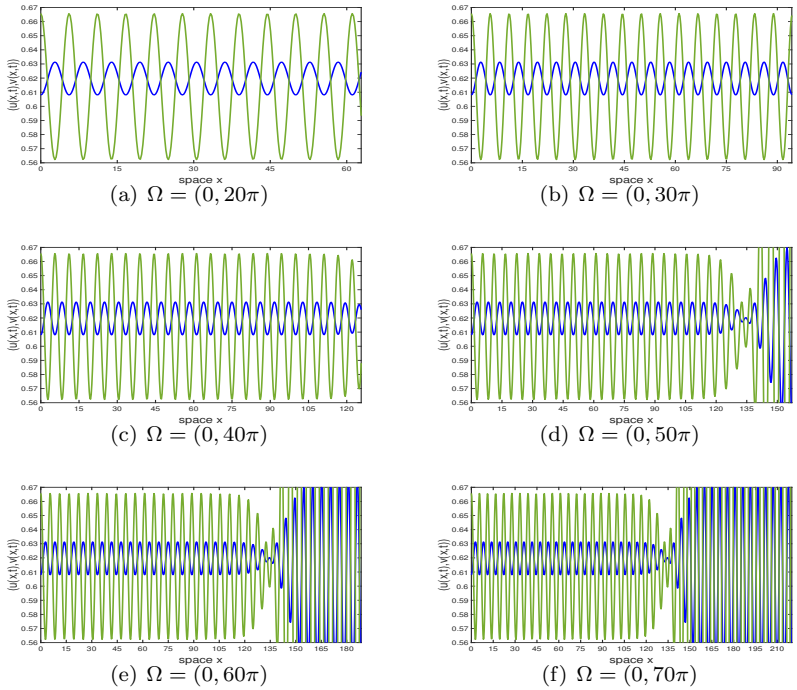

(a) $\Omega = (0, 20\pi)$ (b) $\Omega = (0, 30\pi)$

(c) $\Omega = (0, 40\pi)$ (d) $\Omega = (0, 50\pi)$

(e) $\Omega = (0, 60\pi)$ (f) $\Omega = (0, 70\pi)$

Figure 12. Spatial oscillations of the enzyme-catalyzed system (1) with different scales, where $\alpha = 0.38, \gamma = 2.6, d_1 = 1.65$ and $d_2 = 0.173$.

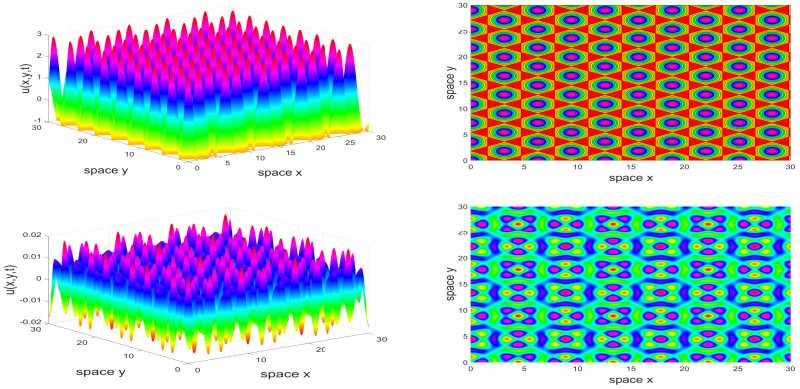

Figure 13. Spatial oscillation of the enzyme-catalyzed system (1) in a two-dimensional domain $\Omega = (0, 30) \times (0, 30)$.

5 Conclusions

In this study, we investigate the spatiotemporal oscillation behavior of an enzyme-catalyzed system under no-flux boundary conditions. We first analyze the stability of the equilibrium and establish the existence of Hopf bifurcation for the diffusion-free system, as detailed in Theorem 1. Since periodic solutions emerge at the Hopf bifurcation point, we derive a stability criterion for these solutions using the multiple time scales (MTS) method. This approach allows us to obtain a concise stability condition, as presented in Theorem 2. When diffusion is introduced, we rigorously analyze the existence of Turing instability, this result is important to find the spatial oscillation of the system. Specifically, we prove the Turing instabilities for equilibrium and bifurcating periodic solution arising from the Hopf bifurcation, as outlined in Theorem 3 and Theorem 4, respectively. These theoretical results confirm the potential for spatiotemporal oscillations in the system. Indeed, numerical simulations reveal distinct oscillation behaviors, including purely temporal, purely spatial, and spatiotemporal oscillations, as illustrated by the snapshot figures in Section 4. In summary, our findings demonstrate that this enzyme-catalyzed model exhibits temporal, spatial, and spatiotemporal oscillations due to the presence of Hopf bifurcation, Turing instability, and Turing-Hopf bifurcation, respectively. We believe that the findings presented herein provide valuable insights into the intricate spatiotemporal dynamics governing the enzyme-catalyzed system. When extending the spatial dimension to two dimensions, for example, setting $\Omega = (0, 30) \times (0, 30)$, the enzyme-catalyzed system (1) exhibits significantly more complex spatial oscillation patterns, as demonstrated in Fig. 13. These higher-dimensional phenomena present intriguing dynamical behaviors that warrant thorough investigation, which we plan to address comprehensively in our future research endeavors.

***Acknowledgment*:** The authors express their sincere thanks to the anonymous reviewers for their comments on revisions. This work was supported by the National Natural Science Foundation of China (No. 12271143), the China Postdoctoral Science Foundation (No. 2021M701118), Key Scientific Research Project of Henan Higher Eduction Institutions

(No. 25A110008), and the Natural Science Foundation of Henan Province (No. 252300420905).

References

[1] M. X. Chen, Pattern dynamics of a Lotka-Volterra model with taxis mechanism, *Appl. Math. Comput.* **484** (2025) #129017.

[2] A. Atabaigi, Turing instabilities in a glycolysis reaction-diffusion system, *Appl. Anal.* **103** (2024) 377–392.

[3] T. Y. Li, Q. R. Wang, Turing patterns in a predator-prey reaction-diffusion model with seasonality and fear effect, *J. Nonlin. Sci.* **33** (2023) #86.

[4] S. Singh, R. C. Mittal, S. R. Thottoli, et al., High-fidelity simulations for Turing pattern formation in multi-dimensional Gray-Scott reaction-diffusion system, *Appl. Math. Comput.* **452** (2023) #128079.

[5] J. Su, Bifurcation analysis of an enzyme reaction system with general power of autocatalysis, *Int. J. Bifurc. Chaos* **29** (2019) #1950079.

[6] W. Ko, Bifurcations and asymptotic behavior of positive steady-states of an enzyme-catalyzed reaction-diffusion system, *Nonlin.* **29** (2016) 3777–3809.

[7] M. Chen, X. Z. Li, Stability analysis and Turing pattern of an enzyme-catalyzed reaction model, *MATCH Commun. Math. Comput. Chem.* **94** (2025) 195–214.

[8] Z. P Ma, J. Z. Han, Global asymptotical stability and Hopf bifurcation for a three-species Lotka-Volterra food web model, *Math. Meth. Appl. Sci.* **48** (2025) 1142–1162.

[9] Y. L. Song, H. P. Jiang, Y. Yuan, Turing-Hopg bifurcation in the reaction-diffusion systen with delay and applixation to a diffusive predator-prey model, *J. Appl. Anal. Comput.* **9** (2019) 1132–1164.

[10] Q. Wang, Y. Song, L. Shao, Nonconstant positive steady states and pattern formation of 1D prey-taxis systems, *J. Nonlin. Sci.* **27** (2017) 71–97.

[11] M. X. Chen, H. M. Srivastava, Existence and stability of bifurcating solution of a chemotaxis model, *Proc. Amer. Math. Soc.* **151** (2023) 4735–4749.

[12] C. F. Liu, S. J. Guo, Steady states of Lotka-Volterra competition models with nonlinear cross-diffusion, *J. Diff. Eq.* **292** (2021) 247–286.

[13] J. Cao, H. Sun, P. Hao, P. Wang, Bifurcation and turing instability for a predator-prey model with nonlinear reaction cross-diffusion, *Appl. Math. Model.* **89** (2021) 1663–1677.

[14] Y. Zhou, X. P. Yan, C. H. Zhang, Turing patterns induced by self-diffusion in a predator-prey model with schooling behavior in predator and prey, *Nonlin. Dyn.* **105** (2021) 3731–3747.

[15] S. Kumari, S. K. Tiwari, R. K. Upadhyay, Cross diffusion induced spatiotemporal pattern in diffusive nutrient-plankton model with nutrient recycling, *Math. Comput. Sim.* **202** (2022) 246–272.

[16] M. Song, S. Gao, C. Liu, Y. Bai, L. Zhang, B Xie, L. Chang, Cross-diffusion induced Turing patterns on multiplex networks of a predator-prey model, *Chaos Solit. Fract.* **168** (2023) #113131.

[17] M. J. Chen, S. M. Fu, Global boundedness and stabilization in a predator-prey model with cannibalism and prey-evasion, *El. J. Quat. Theor. Diff. Eq.* **58** (2023) 1–23.

[18] K. Manna, M. Banerjee, Spatiotemporal pattern formation in a prey-predator model with generalist predator, *Math. Model. Nat. Phen.* **17** (2022) #6.

[19] M. X. Chen, S. Ham, J. Kim, Patterns of a general chemical model involving Degn-Harrison reaction scheme, *MATCH Commun. Math. Comput. Chem.* **93** (2025) 267–290.

[20] B. Anshu, B. Dubey, Spatiotemporal dynamics of a multi-delayed prey-predator system with variable carrying capacity, *Chaos* **33** (2023) #113116.

[21] F. Najm, R. Yafia, M. A. A. Alaoui, Turing bifurcation induced by cross-diffusion and amplitude equation in oncolytic therapeutic model: Viruses as anti-tumor means, *Int. J. Bifur. Chaos* **33** (2023) #2350062.

[22] L. H. Zhu, L. He, Pattern formation in a reaction-diffusion rumor propagation system with Allee effect and time delay, *Nonlin. Dyn.* **107** (2022) 3041–3063.